HHS Public Access

Author manuscript

Phys Med Biol. Author manuscript; available in PMC 2024 July 21.

Published in final edited form as:

Phys Med Biol. ; 68(15): . doi:10.1088/1361-6560/ace23d.

Image-guided focused ultrasound-mediated molecular delivery to breast cancer in an animal model

Ryan Margolis,

Lokesh Basavarajappa,

Junjie Li,

Girgis Obaid,

Kenneth Hoyt

Department of Bioengineering, University of Texas at Dallas, Richardson, TX, USA

Abstract

Tumors become inoperable due to their size or location, making neoadjuvant chemotherapy the primary treatment. However, target tissue accumulation of anticancer agents is limited by the physical barriers of the tumor microenvironment. Low-intensity focused ultrasound (FUS) in combination with microbubble (MB) contrast agents can increase microvascular permeability and improve drug delivery to the target tissue after systemic administration. The goal of this research was to investigate image-guided FUS-mediated molecular delivery in volume space. 3-D FUS therapy functionality was implemented on a programmable ultrasound (US) scanner (Vantage 256, Verasonics Inc) equipped with a linear array for image guidance and a 128-element therapy transducer (HIFUPlex-06, Sonic Concepts). FUS treatment was performed on breast cancer-bearing female mice ($N = 25$). Animals were randomly divided into three groups, namely, 3-D FUS therapy, 2-D FUS therapy, or sham (control) therapy. Immediately prior to the application of FUS therapy, animals received a slow bolus injection of MBs (Definity, Lantheus Medical Imaging Inc) and near-infrared dye (IR-780, surrogate drug) for optical reporting and quantification of molecular delivery. Dye accumulation was monitored via *in vivo* optical imaging at 0, 1, 24, and 48 h (Pearl Trilogy, LI-COR). Following the 48-h time point, animals were humanely euthanized and tumors excised for *ex vivo* analyses. Optical imaging results revealed that 3-D FUS therapy improved delivery of the IR-780 dye by 66.4 and 168.1% at 48 h compared to 2-D FUS ($p = 0.18$) and sham ($p = 0.047$) therapeutic strategies, respectively. *Ex vivo* analysis revealed similar trends. Overall, 3-D FUS therapy can improve accumulation of a surrogate drug throughout the entire target tumor burden after systemic administration.

Keywords

cancer; drug delivery; focused ultrasound; image-guided therapy; microbubble contrast agents; optical imaging

Address correspondence to: Kenneth Hoyt, PhD, MBA, FAIUM, University of Texas at Dallas, BSB 13.929, 800 W Campbell Rd, Richardson, TX 75080 Ph: (972) 883-4958, kenneth.hoyt@utdallas.edu.

1. Introduction

Cancer is a worldwide public healthcare problem. It is the second leading cause of deaths in the United States behind heart disease, with more than 600,000 deaths expected in 2022 (Siegel *et al* 2022). Over the last several decades, there has been a progressive decline in cancer motality due to improved tumor detection and treatment options. The latter involve surgery followed by chemotherapy, with or without radiation therapy. However, surgery is not always an option due to tumor size or location, making neoadjuvant chemotherapy the first line of treatment (Jones *et al* 2020). Numerous clinical studies have concluded that an early response in the neoadjuvant setting is a better prognostic factor of patient survival after surgery than pathological complete response (Montemurro *et al* 2020). If a tumor is responsive, reducing its size before surgery can convert an inoperable cancer to a resectable one (Mieog *et al* 2007). The ability to directly monitor therapeutic efficacy when systemic chemotherapy is given in the neoadjuvant setting is particularly advantageous because there is no measurable disease to follow when the same therapy is given after surgery.

Neoadjuvant systemic therapy is a common approach for the treatment of several different locally advanced or inoperable tumor types, including those of the breast (Wang and Mao 2020), colorectum (Body *et al* 2021), head and neck (Martin 2021), and pancreas (Park *et al* 2021). It has been shown to successfully downgrade inoperable tumors to resectable tumors in roughly 25% of patients diagnosed with colorectal liver metastases (Mestier *et al* 2014) and pancreatic cancer (Strobel *et al* 2012). Furthermore, neoadjuvant chemotherapy has been used extensively to downgrade breast conserving surgery from masectomy to lumpectomy (Wang *et al* 2017). Additional benefits include, but not limited to, increased survival (Mestier *et al* 2014, Wang *et al* 2017, Verhoe *et al* 2011, Chow 2020) and organ preservation (Chow 2020).

The physical microenvironment of cancers present a major challenge to systemic drug delivery in both the neoadjuvant and adjuvant settings. To be most effective, anticancer drugs must penetrate tissue sufficiently, reach all cancer cells in the target population in a concentration sufficient to exert a therapeutic effect (Minchinton and Tannock 2006). However, the abnormal tumor microenvironment can comprise drug efficacy. Unlike the hierachically organized and mature vasculature in healthy tissue, the vasculature within the tumor microenvironment is associated with an overexpression of proangiogenic factors that result in the disorganization and underdevelopment of the blood vessel network (Siemann 2011). More specifically, these immature blood vessels are have inconsistent diameters and shapes attributed to its tortuosity. Furthermore, these structures are dialated and leaky leading to vessel hyperpeameability (Siemann 2011). Overall, the tumor microenvironment is characterized by impaired perfusion, hypoxia, and elevated fluid and solid stresses. After systemic administration, several studies have found that less than 1% of the injected drug dose actually reaches the target tumor site (Rosenblum *et al* 2018, Wilhelm *et al* 2016). To help overcome this drug delivery issue, several groups have explored the use of noninvasive focused ultrasound (FUS) in combination with a microbubble (MB) contrast to safely and reversibly increase permeability of the tumor microvascular barrier (Xiong *et al* 2017, Sirsi and Borden 2014). When exposed to the low-intensity FUS, these intravascular gas-filled MBs undergo stable cavitation (oscillation), which subsequently can exert mechanical

forces that open edothelial gap junctions resulting in enhanced drug extravasation and tumor accumulation (Fig. 1). FUS therapy has also been used to open the blood-brain barrier (Carpentier *et al* 2016, Meng *et al* 2021, Karakatsani *et al* 2017). A recent clinical study evaluated the efficacy of low-intensity FUS in combination with MBs to improve chemotherapeutic efficacy in patients with inoperable pancreatic cancer (Dimcevski *et al* 2016, Kotopoulis *et al* 2013). This initial Phase I clinical trial demonstrated a median survival increase from 8.9 months to 17.6 months in ten subjects augmented with FUS therapy compared to 63 historical controls. Recent efforts to optimize this FUS-mediated drug delivery platform and move forward to a larger Phase II clinical trial has been described (Castle *et al* 2020).

Current FUS therapy approaches include a single element or linear array transducer for delivering the pulsed US exposures to the circulating MBs. In order to treat a larger tissue volume, the transducer must be manually or mechanically displaced. This physical movement can result in poor coupling between the transducer and subject skin, which subsequently makes it more difficult to deliver uniform US exposures to the target tumor tissue. This can be overcome with the use of a FUS therapy system equipped with a three-dimensional (3-D) transducer technology with electronic US beam steering capabilities. While previous research groups have used this approach using custom 2-D arrays (Zhang *et al* 2021, Liu *et al* 2016) for both treatment planning and therapy, we describe a novel US imaged-guided system for FUS-mediated molecular delivery to cancerous tissue in volume space using a commercially available transducer to improve upon previously established 2-D approaches. We hypothesize that this novel 3-D FUS therapeutic approach will improve drug delivery to the targeted tumor tissue as validated by optical imaging.

2. Materials and Methods

2.1 Animal Protocol

Animal experiments were reviewed and approved by the Institutional Animal Care and Use Committee (IACUC) at the University of Texas at Dallas. Breast cancer cells (4T1, American Type Culture Collection, Manassa, VA) were maintained in RPMI-1640 medium with 10% fetal bovine serum (FBS) and 1% penicillin/streptomycin. Cells were cultured at 37°C in a humidified incubator (Heracalle 150i, Thermo Fischer Scientific, Waltham, MA) with 5% CO_2. Cultured cells were numerated using a digital cell counter (Countess II Automated Cell Counter, Thermo Fischer Scientific). Cells were washed twice and resuspended in phosphate buffered saline (PBS, 4.0×10^6 cells/mL). Six-week-old female BALB/c mice ($N = 25$, Charles River Laboratories, Wilmington, MA) were injected with 2.0×10^5 cells into the lower left mammary pad. Experiments began once the implanted tumors reached a size of 8 mm (approximately 10 to 12 days post injection). Mice were randomly divided into three groups, namely, sham therapy ($N = 3$), 2-D US ($N = 9$), or 3-D US ($N = 13$) therapy. During all experimental procedures, mice were placed on a heating pad to maintain a core body temperature and controlled by 1 to 2% isoflurane anesthesia.

2.2 Image-Guided FUS Therapy

Custom 3-D FUS treatment functionality was implemented on a programmable US system (Vantage 256, Verasonics Inc, Kirkland, WA) equipped with a dual transducer configuration (HIFUPlex-06, Sonic Concepts, Bothell, WA) for interleave US imaging and therapy (Basavarajappa and Hoyt 2019). The imaging and therapeutic transducers are both 128-element arrays with center frequencies of 3.5 and 2.0 MHz, respectiviely, attached to a watertight cone for tissue coupling. The latter is a spherically phased array that enables focused US beam steering in volume space. Software on the Vantage 256 system allows implementation of custom FUS treatment protocols via a graphical user interface (GUI) and brightness-modulated (B-Mode) image display of anatomy for defining the treatment area. Basic treatment design used a multi-FUS with temporal sequential excitation (multi-FUS-TSE) (Basavarajappa *et al* 2021). In short, each US focal point is targeted and repeated a specific number of times (referred to as the repetition per focus) before moving to the next focal position. Given all tumors were comparable in size, the number of equally-spaced US focal zones was set constant at 13 and 169 for the 2-D and 3-D multi-FUS-TSE approaches, respectively with 19 repetitions per focal zone for both. The TSE sequence repeated a focal zone 19 times before moving to the next one. Furthermore, application FUS used a pulse repetition frequency of 10 Hz, duty cycle of 10% (10 ms pulse comprised of 3200 cycles) and a peak negative pressure of 0.7 MPa (mechanical index, MI, of 0.45) for a total treatment time of 25 and 320 s for the 2-D and 3-D FUS therapies, respectively. The 2-D and 3-D treatment volumes were 100 and 1298 mm^3 using the focal zone volume of 7.68 mm^3. US parameters were selected based off of previous clinical studies using multi-FUS sequences to improve microvascular permeabilization in volume space (Huang *et al* 2017, Lipsman *et al* 2018, Abrahao *et al* 2019). Transmission gel (Aquasonic 100, Parker Laboratories, Fairfield, NJ) was used to reduce the acoustic impedance mismatch (and air) between the US transducer coupling cone and animal tissue. Immediately prior to all FUS therapeutic sessions, animal was slowly administered a 100 μL bolus solution containing MBs (2.0×10^7 MBs, Definity, Lantheus Medical Imaging, Inc., North Billerica, MA), IR-780 dye (50 μg, Sigma-Aldrich, St Louis, MO), and isotonic saline via a placed tail vein catheter. Control animals received a bolus injection of the same solution under the same physical conditions but received no FUS therapy, which we refer to hereafter as sham therapy.

2.3 Acoustic Measurements

Validation experiments were performed to visualize the custom FUS beam patterns in 3-D sapce. The US beam patterns were measured using calibrated hydrophone scanning system (AIMS III, Onda Corp, Sunnyvale, CA). For simplicity, the hydrophone system measured the therapeutic US transducer output and spatially recorded the peak negative US pressure distribution for each focal zone. Each focal zone had a dimension of $8.0 \times 0.8 \times 1.2$ mm at −3 dB. All focal measures were then combined via summation to produce the composite multi-FUS-TSE treatment plan.

2.4 Optical Imaging

In this study, IR-780 dye was a fluorescent reporter used as a small molecule surrogate drug. To longitudinally monitor IR-780 dye accumulation using the Pearl Trilogy system (LI-COR Bioscience, Lincoln, NE) at baseline (0 h) and again at 1 h, 24 h, and 48 h following FUS or sham therapy. Fluorescent images in live animals were acquired using an 800 nm channel with an excitation and emission filter of 785 and 820 nm, respectively. Registered white light images were also collected for subject visualization and fluorescent image intensity overaly. Using vendor softare (Image Studio Software, LI-COR Bioscience), user-defined region-of-interests (ROIs) were drawn around the tumor circumference and abdominal regions (background signal) under guidance of the white light images. Mean fluorescent image intensity was measured for each ROI.

Following the *in vivo* data acquisition at the 48 h experimental time point, all animals were humanely euthanized via isofluorane overdose followed by cervical dislocation. Tumors were surgically excised and cut in half. One half was used for *ex vivo* optical imaging (Odyssey CLx, LI-COR Biosciences) using excitation and emission filters of 785 and 820 nm, respectively. Quantitative analysis of *ex vivo* fluorescent images followed the *in vivo* protocol. The remaining portion of the excised tumor was preserved for IR-780 dye extraction.

2.5 Optical Dye Extraction

Using a protocol described previously (Xiong *et al* 2017), dedicated excised tumor samples were further cut into fine small pieces, rinsed with saline, and weighed using a digital scale. The tumor pieces were then rinsed again with 1 mL of radio-immunoprecipitation assay buffer and placed in 2 mL tubes with ceramic beads. This buffer was comprised of 50 mM Tris-Base (pH 7.4), 150 mM sodium chloride (NaCl), 1% Triton X-100, 0.5% sodium deoxycholate, and 0.1% sodium dodecyl sulfate (SDS). The ceramic tubes were exposed to high force tissue homogenization (Bead Mill 4 Homogenizer, Thermo Fischer Scientific) for dye extraction followed by centrifugation at 200 g for 10 minutes (repeated twice). Upon completion, 200 μL of supernatant from each tube was transferred into a 96 black well plate and compared against controls of saline and known IR-780 concentrations. Samples were measured in triplicate using a microplate reader (Synergy H4, Bio Tek, Winooski, VT) with an optical excitation at 735 nm and an emission range from 780 to 820 nm. The maximum fluorescent signal in the emission range was used for analysis. Tumor accumulation of IR-780 dye was calculated as the percentage of dye within each tumor tissue sample relative to total dye injection. This value was normalized relative to tumor weight.

2.6 Performance Measures

Group data was summarized as mean ± standard error of the mean. Comparisons of *in vivo* and *ex vivo* analysis were made between the 3-D, 2-D, and sham FUS therapy groups. A Shapiro-Wilks test was performed to assess normality. A Welch's t-test was used to assess time-matched differences in the *in vivo* and *ex vivo* fluorescent images of the tumor tissue. A Kruskal-Wallis test was used to analyze the tumor volume at 0 h and tumor weight at 24 h for the different experimental group measurements. A p-value of less than 0.05 was

considered statistically significant. All statistical analyses were performed using Prism 9.3 (GraphPad Software Inc., San Diego, CA).

3. Results

An US image-guided multi-FUS-TSE therapeutic system and method was developed using a programmable US scanner. Software and a GUI interface allows personalization of the treatment plan throughout a user-defined ROI before extrapolation to volume space. A representative composite 30D FUS beampattern as mapped using measurements from a hydrophone system is presented in Fig. 3. While there is some noticeable spatial aberration in these orthogonal views due to sidelobe activity, the peak negative US pressure distribution is near spatially uniform throughout the focal region.

A preclinical study assessed multi-FUS-TSE treatment using both 2-D and 3-D approaches and cancer-bearing animals. An initial measurement of group tumor sizes at baseline confirmed all were approximately the same in size. The average tumor volumes for the sham, 2-D, and 3-D groups were 321.2 ± 138.6 mm^3, 236.9 ± 138.8 mm^3, and 344.0 ± 199.7 mm^3, respectively (Fig. 4, $p = 0.54$). Animals then received an intravenous bolus injection of a MB and IR-780 dye solution immediately before application of FUS or sham therapy to the tumor mass. *In vivo* optical images were acquired at baseline before therapy and again at 1, 24, and 48 h to monitor fluorescent dye accumulation in the target tissue. Mean image intensity values were extracted and normalized with respect to the abdomen region signal intensity and ROI size. As revealed by inspection of Fig. 5, there was a noticeable progressive accumulation of the optical dye throughout the 48-h experimental window. Moreover, it qualitatively appears that 3-D FUS therapy results in an increased intratumoral optical image intensity compared to both 2-D FUS and sham therapy. Note that changes in the sham therapy group mice were attributed to passive accumulation of the optical dye due to an enhanced permeability and retention (EPR) effect. A summary of all optical image measurements is summarized in Fig. 6. These quantitative group findings confirm that application of 3-D FUS therapy results in higher tumor fluorescent signal measurements after 24 and 48 h as compared to those from animals that received 2-D FUS ($p = 0.18$) or sham therapy ($p = 0.047$). More specifically, intratumoral IR-780 dye accumulation after use of 3-D FUS therapy was 66.4 and 168.1% higher at 48 h when compared to use of 2-D FUS or sham therapy, respectively.

After the last optical imaging time point, animals were humanely euthanized, and tumors excised for *ex vivo* analysis. Note that the weight of tumor samples from all groups were comparable ($p = 0.50$), Fig. 7(a). Each tumor was then sectioned along the maximum diameter and used for either *ex vivo* optical imaging or homogenization and IR-780 dye extraction. Representative high-resolution optical images and a summary of fluorescent image intensity for each animal group is represented in Fig. 7(b). Note the increased IR-780 dye localization in tissue exposed to 2-D or 3-D FUS therapy. Quantitative analysis of fluorescent image intensity reveals that the use of 2-D and 3-D FUS therapy produced significantly higher levels of IR-780 compared to sham therapy measures ($p < 0.02$). Normalized fluorescent signals after extraction of any accumulated IR-780 dye from the tumor tissue exhibited a similar trend as shown in Fig. 7(c), showing increased accumulation

in mice treated with 3-D FUS therapy over 2-D ($p = 0.53$) and sham ($p = 0.12$) strategies. Collectively, these preclinical experimental results support the claim that 3-D multi-FUS-TSE-mediated drug delivery could improve accumulation in the target tumor volume compared to 2-D or sham therapy approaches.

4. Discussion

This research study introduced a novel low-intensity 3-D multi-FUS-TSE system that was shown to considerably increase surrogate drug accumulation in cancer tissue compared to a previously established 2-D therapeutic approach (Basavarajappa *et al* 2021). This prior study established a custom pulse sequence for applying FUS treatment in 2-D space by investigating the effect on systemic extravasation of an optical reporter in targeted tissue. The treatment sequences assessed were multi-FUS with sequential excitation (multi-FUS-SE) and multi-FUS with temporal sequential excitation (multi-FUS-TSE) approaches. The multi-FUS-SE sequence targeted different focal positions in a sequenced fashion before being repeated a specific number of times, whereas the multi-FUS-TSE approach repeats each focal zone a specific number of times before moving to the next focal position. Previous research demonstrated that the multi-FUS-TSE sequence improved delivery of a systemically administered optical reporter to target tumor tissue by 36 and 50% compared to the multi-FUS-SE ($p = 0.28$) and single-FUS ($p = 0.22$) therapy approaches, respectively (Basavarajappa *et al* 2021). The same procedure for optical dye extraction from excised tumor samples used in this study confirmed higher surrogate drug accumulation in the tumor tissue after multi-FUS-TSE treatment compared to multi-FUS-SE and sham therapies. The research presented in this study further expanded on previous research by extrapolating the multi-FUS-TSE sequence to 3-D space and treatment of the entire tumor volume. Preliminary data was previously published and demonstrated an increase in drug accumulation in mice treated with 3-D FUS therapy compared to a 2-D appraoch ($p < 0.03$) (Margolis *et al* 2021). The full cohort followed a similar trend, albeit not statistically significant. The 3-D multi-FUS-TSE approach showed average optical dye enhancement increases of 250 and 160% compared to the 2-D and sham therapy approaches, respectively. Discrepancies between the preliminary data and full cohort could be attributed to several factors such as variations in abdominal signal, temperature, and treatment volumes. However, increased treatment time of the 3-D FUS therapy and limited circulation time of the MBs are counterproductive, meaning that towards the end of treatment there may have been little or no MBs in circulation. The 3-D FUS treatment stimulates a larger tissue volume than the 2-D FUS approach. This leads to a higher abdominal signal and reference from where the tumor signal intensity is measured. The average optical image intensities from the abdomen were at least 30 and 94% higher for mice treated with 3-D FUS therapy at 24 and 48 h when compared to the 2-D and sham FUS therapies, respectively. The increase in vasolidation, which is in part due to the larger treatment volume, could account for the increased abdomen signal. Furthermore, this increase in signal could be due to temperature increase caused by the 3-D FUS therapy, which will need to be monitored for treatment optimization. The image-guidance for FUS therapy was performed in 2-D space. However, since we were unable to visualize the alignment in 3-D, the treatment volume could be off by 1 to 2 mm at – 3 dB in its orthogonal direction. This could explain the dye accumulation

in the surrounding tissue outside the treatment region, but also the reduced signal within the tumor volume. The respiration motion of the mouse could potentially enhance these effects. Furthermore, necrosis was more common in mice treated with the 3-D FUS therapy as compared to the 2-D appraoch. This might account for optical signal variation at the lower values among mice treated with 3-D FUS. A research study showed that the 4T1 cell line is associated with extensive necrosis 10 wk post implantation (Tao *et al* 2008). The 3-D FUS treatment could have accelerated necrosis within the tumor.

Following the 48 h time point, tumors were place in formalin for 24 h. During this time, it's possible some of the optical dye leaked or was exposed to light. Both would reduce the optical signal. The increase in necrotic tissue could also minimize the increase in dye accumulation in the tumors treated with 3-D FUS therapy. The waiting time for the dye extraction process increased the stiffness of the tumor pieces during the tissue homogenization step for optical dye extraction, which required the tumor tissue to be sliced into smaller pieces. The inability to completely homogenize the tumor tissue could account for optical images from the 2-D and 3-D FUS therapy group mice being notably different but not statically significant.

Recent work by Gong *et al*. investigated these same FUS sequences for improved delivery of a monclonal antibody directed against programmed cell death ligand 1 (anti-PD-L1) over a large volume in the brain (Gong *et al* 2022). The multi-FUS-SE and multi-FUS-TSE approaches that were investigated found that the interleaved temporal sequence performed better than the serial sequence by 1.3-fold ($p > 0.05$). While these collective results are promising, customization of the 3-D multi-FUS-TSE approach to be more subject specific could further improve delivery of systemically administered therapy.

Future customization of our 3-D FUS system will investigate both US parameters and MB properties (Sorace *et al* 2012, McDannold *et al* 2008). This stable cavitation is associated with mechanical bioeffects like improved blood flow and tissue oxygenation, reduced interstial fluid pressures, and increased microvascular permeability (Joiner *et al* 2020, Zhang *et al* 2019). A strategic innovation could be maximizing (exploiting) these physical changes when desirable. FUS parameters like pulse repetition frequency, pulse duration, and duty cycle, will be varied and correlated to the desired target effect of maximal drug extravasation. Tailoring FUS applications to specific tumor sizes by controlling the number of focal positions and repetitions per focal zone would maximize the spatial effect of FUS therapy and minimize bioeffects to healthy tissue. This would require establishing a uniform exposure pattern while keeping treatment time to as low as reasonably achievable (ALARA). Therapy planning software should be configured to automate the treatment protocol for specific tumor dimensions.

3-D FUS requires an extensive treatment window to achieve sufficient drug delivery throughout the entire tumor volume (on order of minutes). Therefore, MB dosing schedule and impact of MB size should be revisited (Choi *et al* 2010, McMahon and Hynynen 2017). Studies have shown that liposomes with particles sizes from 100 to 200 nm can accumulate agent concentration four times greater than particles sizes smaller than 50 nm or larger than 300 nm in tumors following low-intensity focused ultrasound (He *et al* 2022).

It was intimated that larger MBs have a higher likelihood to increase permeability in the microvascular network (e.g., capillaries that are 8 to 10 μm in diameter), whereas smaller contrast agents in circulation may not come in contact with the microvascular walls as often as needed to induce the desired therapeutic effect.

Success of FUS therapy is dependent on the presence of intravascular MBs in the target tissue. While slow bolus injections are standard practice for MB administration (Xiong *et al* 2017, Basavarajappa *et al* 2021, Margolis *et al* 2021), dynamic influx and clearance mechanisms prevent delivery of a uniform dose with time. Therefore, continuous MB infusions could potentially improve FUS therapeutic outcomes. Recent research has demonstrated successful BBB disruption using a continuous infusion of commerical MBs and FUS applied to multiple focal positions (Lapin *et al* 2020). Using magnetic resonance imaging (MRI) contrast enhancement rate as a target metric, it was found that FUS therapy and MB infusions at 7.2 μL/kg/min or below produced consistent BBB opening. However, when infusion rates exceeded 20 μL/kg/min, signs of tissue injury occurred at higher US pressures. When compared to FUS therapy using a bolus MB injection, it was concluded that MB infusion offers a more controlled and consistent approach for performing multi-FUS therapy. Thus, a decrease in MB concentration at the end of the 3-D therapy could result in a reduced microvacular permeability, minimizing the effect of the 3-D therapy.

Needle size and flow rate has a profound impact on MB administration and could negatively imapct FUS therapy if not carefully considered. Previous research investigated the role of needle and catheter size on the reproducibility of MB injections (Eisenbrey *et al* 2015). As compared to use of 18, 20, and 21G needles, it was found that use of a smaller bore 25G needle resulted in considerable MB rupture during dosing ($p < 0.001$). Our research protocol involved use of a 27G needle for proper tail vein access and injections, so MB concentration could have decreased during FUS treatment contributing to procedure variance. Combined with inconsistencies in MB distribution throughout each focal zone during use of bolus injections, future investigations will revisit the MB delivery protocol.

The current study used US image guidance to determine treatment location so only target tissue was treated. A more informative technique to monitor FUS treatment should minimize off-target effects and treatment time. To accomplish this, a technique that monitors backscattered US signals during MB cavitation using a real-time feedback loop could be beneficial (Vignon *et al* 2013). This allows application of FUS therapy during stable MB cavitation while avoiding inertial cavitation and creation of undesired bioeffects (Miller *et al* 2008). One strategy involves passive cavitation detection that would provide an improved FUS treatment window for maximum therapuetic effect. The mathematical algorithms behind these methods have been extensively studied. The delay, sum, and integrate approach was successfully implemented *in vitro* using custom albumin-coated MBs exposed to 2 MHz US pulses at various peak negative pressures to produce ultraharmonic and broadband emissions (Haworth *et al* 2017). Another study investigated the use of the robust Capon beamformer for improved cavitation mapping owing to decreased spurious artifacts (Coviello *et al* 2015). Chien *et al.* successfully implemented a closed-loop feedback control for FUS-mediated BBB opening (Chien *et al* 2022). This study showed that BBB opening was safely achieved using passive cavitation detection at various MB cavitation levels.

Moreover, passive cavitation imaging was successfully used to monitor the spatiotemporal MB activity (Yang *et al* 2019). The use of passive cavitation imaging was used to validate the advantagess of FUS exposure patterns for inducing BBB opening throughout a larger tissue volume (Gong *et al* 2022). These techniques are sustainable as long as there are sufficient MBs in circulation to create backscattered US signals. Another possible opportunity to control FUS treatment would be to monitor spatiotemporal properties of the FUS beampattern to help maintain proper focal positioning on the target tissue (Thies and Oelze 2021).

5. Conclusion

A 3-D multi-FUS-TSE therapeutic approach was introduced and shown to improve systemic delivery of surrogate drugs to target cancerous tissue over the pre-existing 2-D and sham therapies. While preliminary findings are encouraging, FUS treatment protocols need to be further customized and tailored to varying tumor shapes. Implementation of real-time feedback control to monitor MB cavitation will help maximize FUS therapeutic outcomes.

References

Abrahao A, Meng Y, Llinas M, Huang Y, Hamani C, Mainprize T, Aubert I, Heyn C, Black SE, Hynynen K, Lipsman N and Zinman L 2019 First-in-human trial of blood–brain barrier opening in amyotrophic lateral sclerosis using MR-guided focused ultrasound Nat Commun 10 4373 [PubMed: 31558719]

Basavarajappa L and Hoyt K 2019 Image-guided focused ultrasound therapy system and method for improved anticancer drug delivery Proc IEEE Ultrason Symp 1 2428–31

Basavarajappa L, Rijal G and Hoyt K 2021 Multifocused ultrasound therapy for controlled microvascular permeabilization and improved drug delivery IEEE Trans Ultrason Ferroelectr Freq Control 68 961–8 [PubMed: 32976098]

Body A, Prenen H, Latham S, Lam M, Tipping-Smith S, Raghunath A and Segelov E 2021 The role of neoadjuvant chemotherapy in locally advanced colon cancer Cancer Manag Res 13 2567–79 [PubMed: 33762848]

Carpentier A, Canney M, Vignot A, Reina V, Beccaria K, Horodyckid C, Karachi C, Leclercq D, Lafon C, Chapelon J-Y, Capelle L, Cornu P, Sanson M, Hoang-Xuan K, Delattre J-Y and Idbaih A 2016 Clinical trial of blood-brain barrier disruption by pulsed ultrasound Sci. Transl. Med. 8

Castle J, Kotopoulis S and Forsberg F 2020 Sonoporation for augmenting chemotherapy of pancreatic ductal adenocarcinoma Methods Mol Biol 2059 191–205 [PubMed: 31435922]

Chien C-Y, Yang Y, Gong Y, Yue Y and Chen H 2022 Blood-brain barrier opening by individualized closed-loop feedback control of focused ultrasound BME Frontiers 2022 9867230

Choi JJ, Feshitan JA, Baseri B, Wang S, Tung Y-S, Borden MA and Konofagou EE 2010 Microbubble-size dependence of focused ultrasound-induced blood-brain barrier opening in mice in vivo IEEE Trans Biomed Eng 57 145–54 [PubMed: 19846365]

Chow LQM 2020 Head and neck cancer ed D L Longo N Engl J Med 382 60–72 [PubMed: 31893516]

Coviello C, Kozick R, Choi J, Gyöngy M, Jensen C, Smith PP and Coussios C-C 2015 Passive acoustic mapping utilizing optimal beamforming in ultrasound therapy monitoring J Acoust Soc Am 137 2573–85 [PubMed: 25994690]

Dimcevski G, Kotopoulis S, Bjånes T, Hoem D, Schjøtt J, Gjertsen BT, Biermann M, Molven A, Sorbye H, McCormack E, Postema M and Gilja OH 2016 A human clinical trial using ultrasound and microbubbles to enhance gemcitabine treatment of inoperable pancreatic cancer J Control Release 243 172–81 [PubMed: 27744037]

Eisenbrey JR, Daecher A, Kramer MR and Forsberg F 2015 Effects of needle and catheter size on commercially available ultrasound contrast agents J Ultrasound Med 34 1961–8 [PubMed: 26384606]

Gong Y, Ye D, Chien C-Y, Yue Y and Chen H 2022 Comparison of sonication patterns and microbubble administration strategies for focused ultrasound-mediated large-volume drug delivery IEEE Trans Biomed Eng

Haworth KJ, Bader KB, Rich KT, Holland CK and Mast TD 2017 Quantitative frequency-domain passive cavitation imaging IEEE Trans Ultrason Ferroelectr Freq Control 64 177–91 [PubMed: 27992331]

He J, Liu Z, Zhu X, Xia H, Gao H and Lu J 2022 Ultrasonic microbubble cavitation enhanced tissue permeability and drug diffusion in solid tumor therapy Pharmaceutics 14 1642 [PubMed: 36015267]

Huang Y, Alkins R, Schwartz ML and Hynynen K 2017 Opening the blood-brain barrier with MR imaging–guided focused ultrasound: Preclinical testing on a trans–human skull porcine model Radiology 282 123–30 [PubMed: 27420647]

Joiner JB, Pylayeva-Gupta Y and Dayton PA 2020 Focused ultrasound for immunomodulation of the tumor microenvironment J Immunol 205 2327–41 [PubMed: 33077668]

Jones EF, Hathi DK, Freimanis R, Mukhtar RA, Chien AJ, Esserman LJ, van't Veer L J, Joe BN and Hylton NM 2020 Current landscape of breast cancer imaging and potential quantitative imaging markers of response in ER-positive breast cancers treated with neoadjuvant therapy Cancers 12 1511 [PubMed: 32527022]

Karakatsani MEM, Samiotaki GM, Downs ME, Ferrera VP and Konofagou EE 2017 Targeting effects on the volume of the focused ultrasound-induced blood-brain barrier opening in nonhuman primates in vivo IEEE Trans Ultrason Ferroelectr Freq Control 64 798–810 [PubMed: 28320656]

Kotopoulis S, Dimcevski G, Gilja OH, Hoem D and Postema M 2013 Treatment of human pancreatic cancer using combined ultrasound, microbubbles, and gemcitabine: a clinical case study Med Phys 40 072902 [PubMed: 23822453]

Lapin NA, Gill K, Shah BR and Chopra R 2020 Consistent opening of the blood brain barrier using focused ultrasound with constant intravenous infusion of microbubble agent Sci Rep 10 16546 [PubMed: 33024157]

Lipsman N, Meng Y, Bethune AJ, Huang Y, Lam B, Masellis M, Herrmann N, Heyn C, Aubert I, Boutet A, Smith GS, Hynynen K and Black SE 2018 Blood–brain barrier opening in Alzheimer's disease using MR-guided focused ultrasound Nat Commun 9 2336 [PubMed: 30046032]

Liu J, Foiret J, Stephens DN, Le Baron O and Ferrara KW 2016 Development of a spherically focused phased array transducer for ultrasonic image-guided hyperthermia Phys. Med. Biol. 61 5275–96 [PubMed: 27353347]

Margolis R, Basavarajappa L, Li J and Hoyt K 2021 Ultrasound image-guided drug delivery using a spherically focused phased array transducer Proc IEEE Ultrason Symp 1 1–4

Martin JT 2021 Consolidation therapy in esophageal cancer Surg Clin North Am 101 483–8 [PubMed: 34048767]

McDannold N, Vykhodtseva N and Hynynen K 2008 Blood-brain barrier disruption induced by focused ultrasound and circulating preformed microbubbles appears to be characterized by the mechanical index Ultrasound Med Biol 34 834–40 [PubMed: 18207311]

McMahon D and Hynynen K 2017 Acute inflammatory response following increased blood-brain barrier permeability induced by focused ultrasound is dependent on microbubble dose Theranostics 7 3989–4000 [PubMed: 29109793]

Meng Y, Hynynen K and Lipsman N 2021 Applications of focused ultrasound in the brain: From thermoablation to drug delivery Nat Rev Neurol 17 7–22 [PubMed: 33106619]

Mestier L de, Manceau G, Neuzillet C, Bachet JB, Spano JP, Kianmanesh R, Vaillant JC, Bouché O, Hannoun L and Karoui M 2014 Primary tumor resection in colorectal cancer with unresectable synchronous metastases: A review WJGO 6 156 [PubMed: 24936226]

Mieog JSD, van der Hage JA and van de Velde CJH 2007 Neoadjuvant chemotherapy for operable breast cancer British Journal of Surgery 94 1189–200 [PubMed: 17701939]

Miller DL, Averkiou MA, Brayman AA, Everbach EC, Holland CK, Wible JH and Wu J 2008 Bioeffects considerations for diagnostic ultrasound contrast agents J Ultrasound Med 27 611–32 [PubMed: 18359911]

Minchinton AI and Tannock IF 2006 Drug penetration in solid tumours Nat Rev Cancer 6 583–92 [PubMed: 16862189]

Montemurro F, Nuzzolese I and Ponzone R 2020 Neoadjuvant or adjuvant chemotherapy in early breast cancer? Expert Opinion on Pharmacotherapy 21 1071–82 [PubMed: 32237920]

Park W, Chawla A and O'Reilly EM 2021 Pancreatic Cancer: A review JAMA 326 851 [PubMed: 34547082]

Rosenblum D, Joshi N, Tao W, Karp JM and Peer D 2018 Progress and challenges towards targeted delivery of cancer therapeutics Nat Commun 9 1410 [PubMed: 29650952]

Siegel RL, Miller KD, Fuchs HE and Jemal A 2022 Cancer statistics, 2022 CA A Cancer J Clinicians 72 7–33

Siemann DW 2011 The unique characteristics of tumor vasculature and preclinical evidence for its selective disruption by Tumor-Vascular Disrupting Agents Cancer Treatment Reviews 37 63–74 [PubMed: 20570444]

Sirsi SR and Borden MA 2014 State-of-the-art materials for ultrasound-triggered drug delivery Adv Drug Deliv Rev 72 3–14 [PubMed: 24389162]

Sorace AG, Warram JM, Umphrey H and Hoyt K 2012 Microbubble-mediated ultrasonic techniques for improved chemotherapeutic delivery in cancer J Drug Target 20 43–54 [PubMed: 21981609]

Strobel O, Berens V, Hinz U, Hartwig W, Hackert T, Bergmann F, Debus J, Jäger D, Büchler MW and Werner J 2012 Resection after neoadjuvant therapy for locally advanced, "unresectable" pancreatic cancer Surgery 152 S33–42 [PubMed: 22770956]

Tao K, Fang M, Alroy J and Sahagian GG 2008 Imagable 4T1 model for the study of late stage breast cancer BMC Cancer 8 228 [PubMed: 18691423]

Thies M and Oelze ML 2021 Real-time visualization of a focused ultrasound beam using ultrasonic backscatter IEEE Trans Ultrason Ferroelectr Freq Control 68 1213–23 [PubMed: 33147143]

Verhoe C, de Wilt J H, Burger JWA, Verheu HMW and Koopman M 2011 Surgery of the primary in stage IV colorectal cancer with unresectable metastases European Journal of Cancer 47 S61–6 [PubMed: 21944031]

Vignon F, Shi WT, Powers JE, Everbach EC, Liu J, Gao S, Xie F and Porter TR 2013 Microbubble cavitation imaging IEEE Trans Ultrason Ferroelectr Freq Control 60 661–70 [PubMed: 23549527]

Wang H and Mao X 2020 Evaluation of the efficacy of neoadjuvant chemotherapy for breast cancer Drug Des Devel Ther 14 2423–33

Wang M, Hou L, Chen M, Zhou Y, Liang Y, Wang S, Jiang J and Zhang Y 2017 Neoadjuvant chemotherapy creates surgery opportunities for inoperable locally advanced breast cancer Sci Rep 7 44673 [PubMed: 28327615]

Wilhelm S, Tavares AJ, Dai Q, Ohta S, Audet J, Dvorak HF and Chan WCW 2016 Analysis of nanoparticle delivery to tumours Nat Rev Mater 1 16014

Xiong F, Nirupama S, Sirsi SR, Lacko A and Hoyt K 2017 Ultrasound-stimulated drug delivery using therapeutic reconstituted high-density lipoprotein nanoparticles Nanotheranostics 1 440–9 [PubMed: 29188177]

Yang Y, Zhang X, Ye D, Laforest R, Williamson J, Liu Y and Chen H 2019 Cavitation dose painting for focused ultrasound-induced blood-brain barrier disruption Sci Rep 9 2840 [PubMed: 30808897]

Zhang Q, Jin H, Chen L, Chen Q, He Y, Yang Y, Ma S, Xiao S, Xi F, Luo Q and Liu J 2019 Effect of ultrasound combined with microbubble therapy on interstitial fluid pressure and VX2 tumor structure in rabbit Front Pharmacol 10 716 [PubMed: 31293427]

Zhang Z, Liu R, Li G, Su M, Li F, Zheng H and Qiu W 2021 A dual-mode 2D matrix array for ultrasound image-guided noninvasive therapy IEEE Trans. Biomed. Eng. 68 3482–90 [PubMed: 33872140]

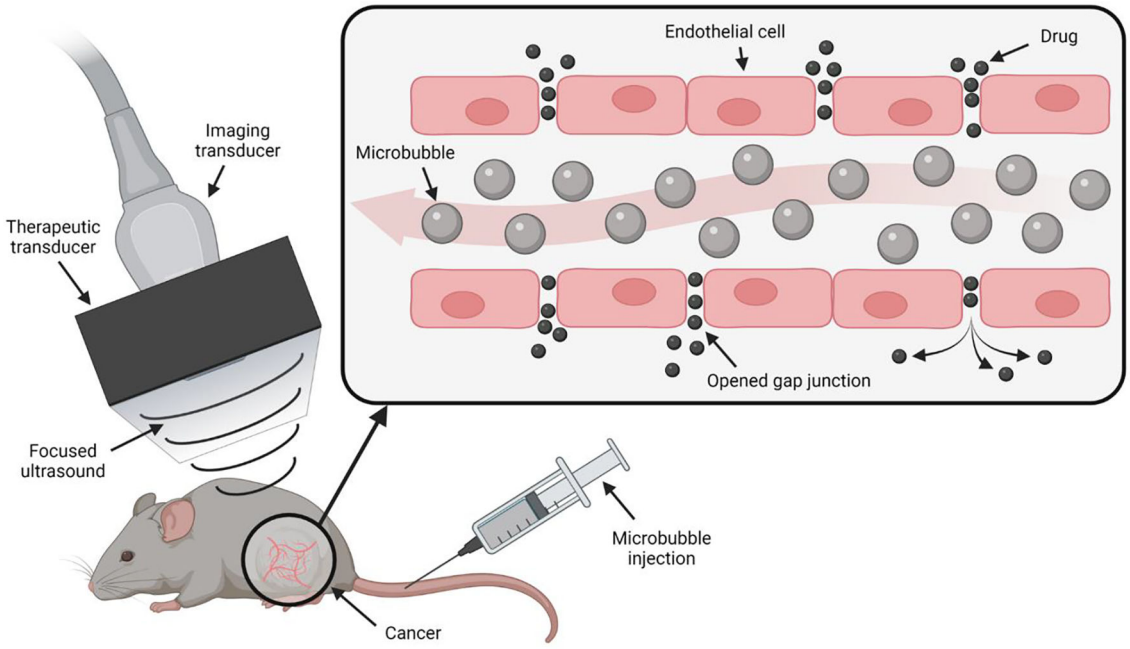

Figure 1. Image-guided focused ultrasound (FUS) and microbubble (MB) interaction for improved systemic drug delivery.

Exposure of intravascular MB contrast agents to low-intensity FUS creates mechanical forces that temporarily induces microvascular permeability for increased delivery of systemic drugs and accumulation in the target tumor tissue.

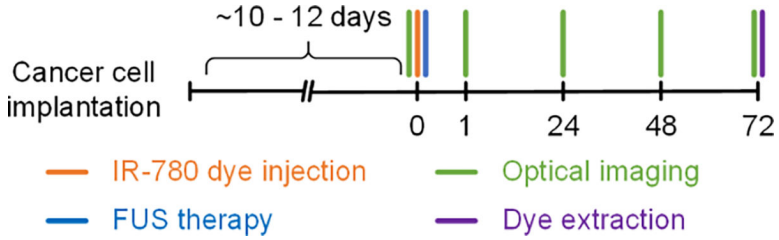

Figure 2. Schematic diagram of the experimental timeline and procedures involving FUS therapy and optical imaging of IR-780 dye.

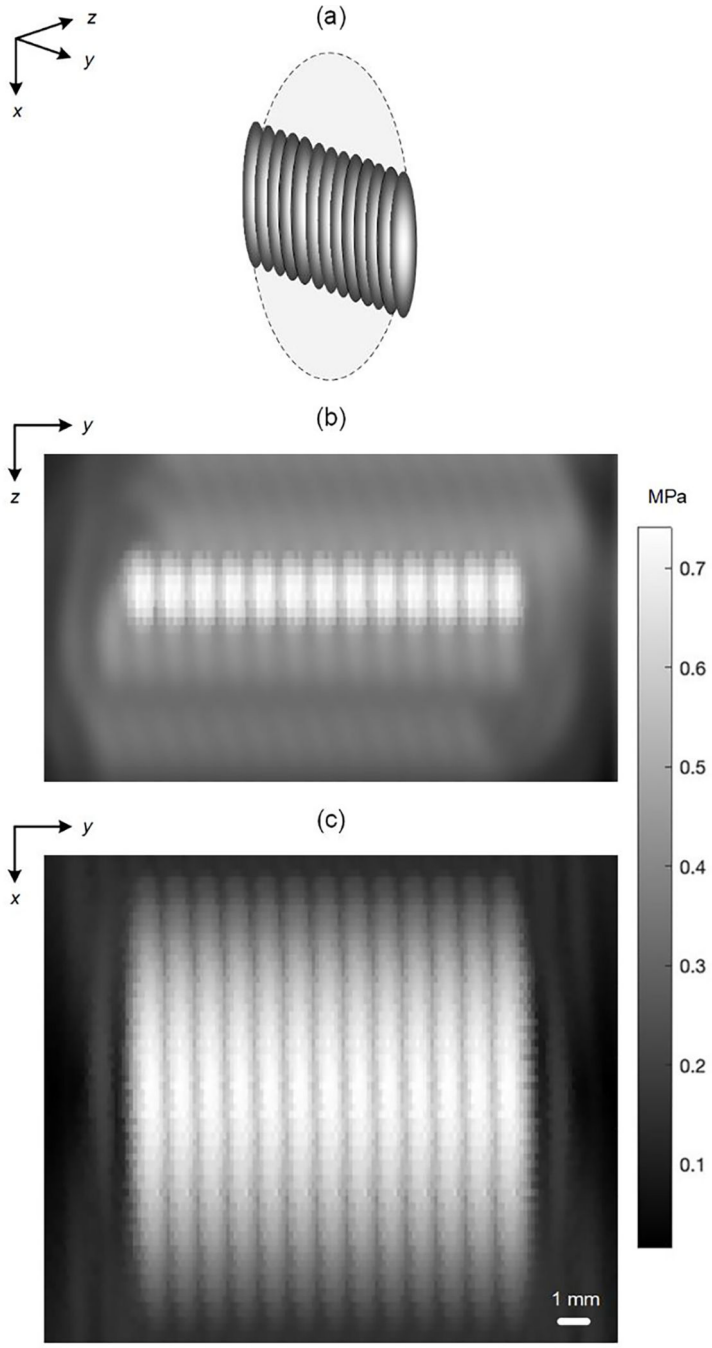

Figure. 3. Experimental mapping of the composite beampattern used for FUS therapy.

FUS treatment was implemented and beampatterns were visualized using a calibrated hydrophone set-up. For simplicity and ease of visualization, only a 2-D FUS treatment plan is displayed. The three-dimensional view of the 2-D approach is seen on the left, showing the 13 focal zones along the middle plane (light gray oval) of the tumor (darker gray circle). These measurements were taken at −3 dB.

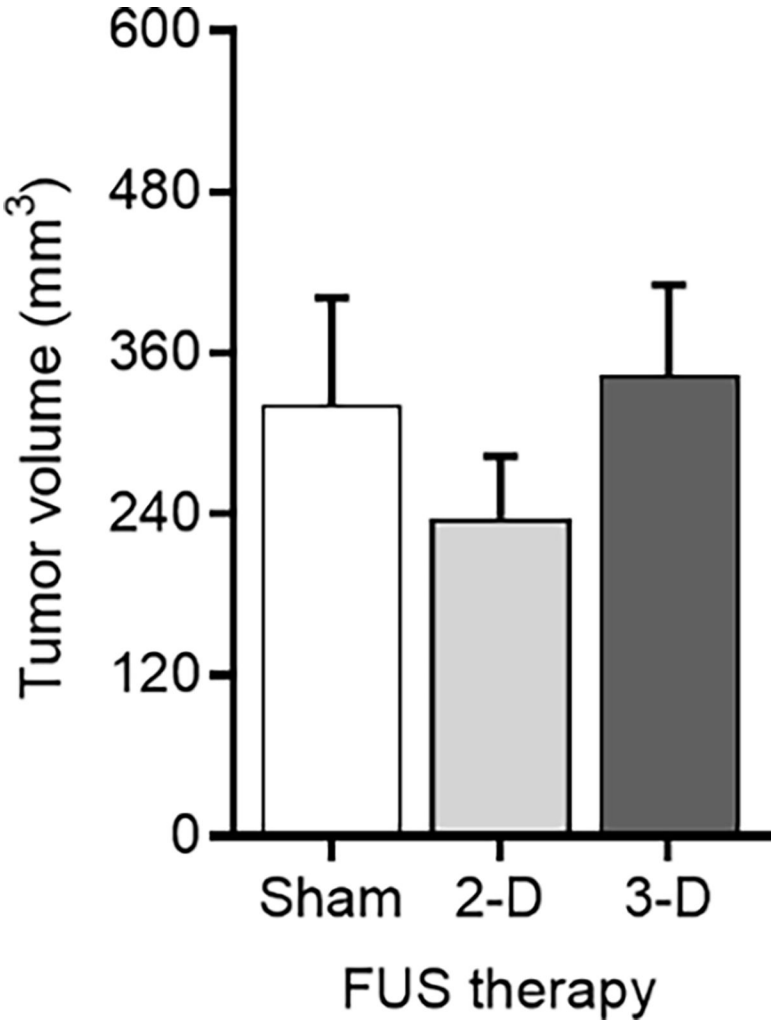

Figure 4. Comparison of tumor volumes used for FUS-mediated molecular delivery.

Animals were randomly divided into FUS or sham therapy groups based on tumor volume measurements. The average tumor volumes for the sham, 2-D, and 3-D groups were measured to be 321.2 ± 138.6 mm^3, 236.9 ± 138.8 mm^3, and 344.0 ± 199.7 mm^3, respectively ($p = 0.54$). Tumor volumes were at least 30 times larger than the focal zone volume.

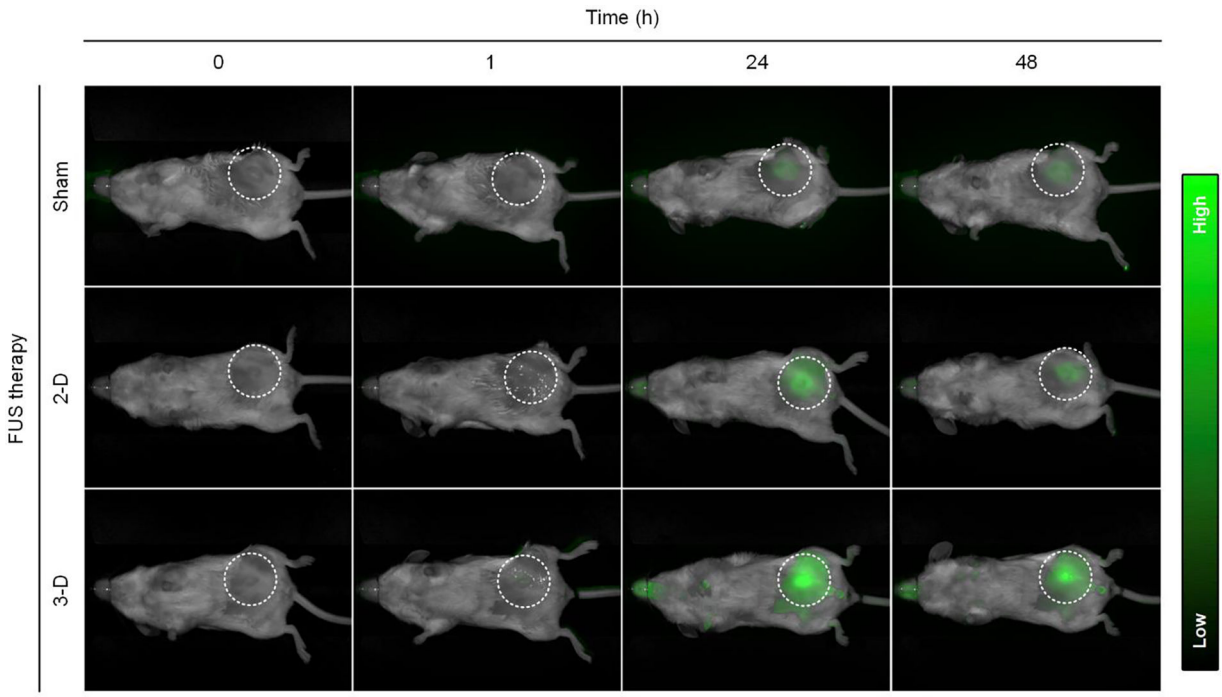

Figure 5. Representative *in vivo* optical images from live cancer-bearing animals that received FUS or sham therapy.

Longitudinal optical images were acquired at baseline before application of a single session of FUS therapy and again at 1, 24, and 48 h thereafter. Note the increased optical dye accumulation in the tumor tissue in mice treated with the 3-D multi-FUS-TSE as compared to the 2-D and sham approaches.

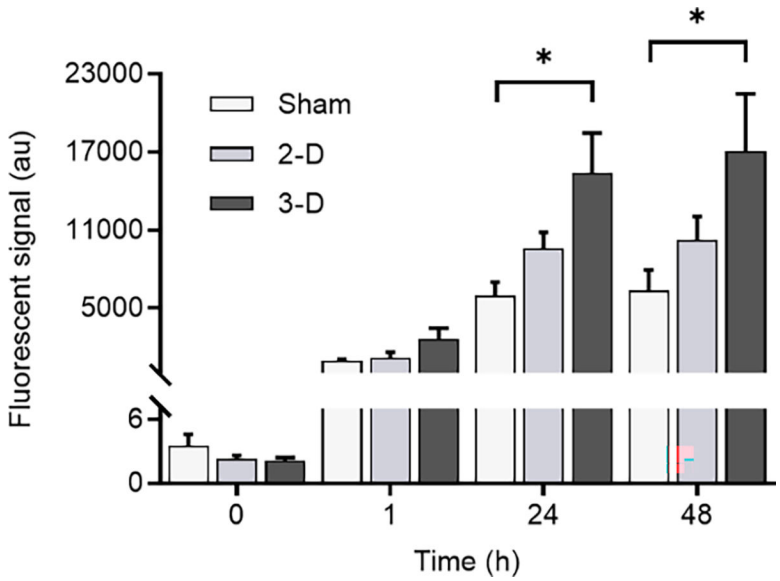

Figure 6. Quantitative summary of *in vivo* optical images.

Optical imaging was used to assess IR-780 dye uptake cancer-bearing animals administrated FUS or sham therapy at baseline, 1, 24, and 48 h. Inspection of data (represented as mean ± standard deviation) reveals that 3-D FUS therapeutic approach significantly increased optical dye retention in the tumor burden at both 24 and 48 h.

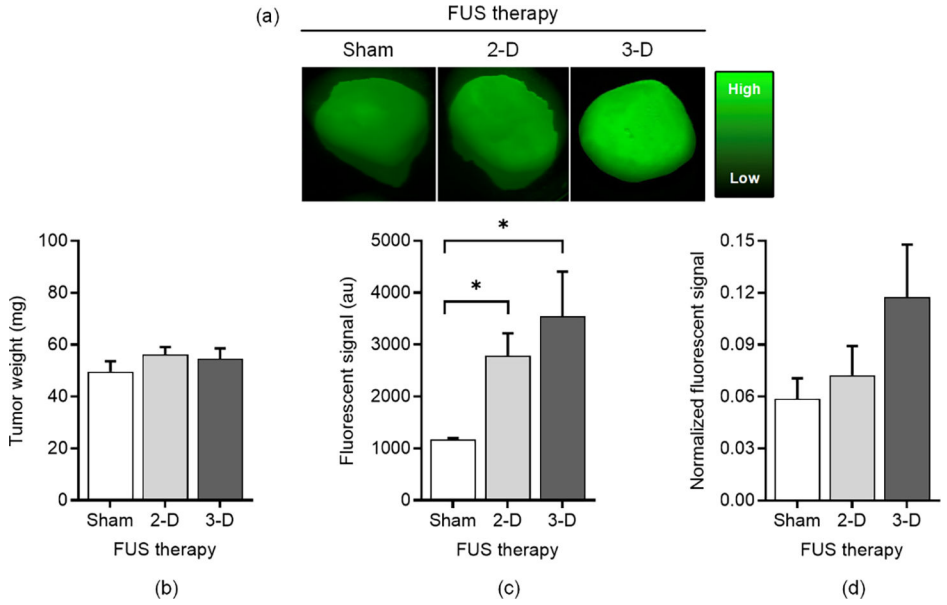

Figure 7. Quantitative analysis of excised tumor samples and *ex vivo* measurements.

(a) Representative *ex vivo* optical images of tumor masses for spatial visualization of the optical dye distribution. (b) Comparison of tumor weights prior to *ex vivo* analysis and after (c) quantitative analysis of *ex vivo* optical images. Note that the 3-D and 2-D FUS approaches significantly increased IR-780 dye accumulation in tumor tissue as confirmed by (d) tissue homogenization for dye extraction and quantification. Dye extraction quantification was normalized by tumor weight.